Title

Understanding the Role of SEI Layer in Low-Temperature Performance of Lithium-Ion Batteries



Journal

ACS Applied Materials & Interfaces, 14(9)

ISSN

1944-8244

Authors

Yoo, Dong-Joo

Liu, Qian

Cohen, Orion

et al.

Publication Date

2022-03-09

DOI

10.1021/acsami.1c23934

# Understanding the Role of SEI Layer in Low-Temperature Performance of Lithium-Ion Batteries

Dong-Joo Yoo,[1,5] Qian Liu,[1] Orion Cohen,[2] Minkyu Kim,[1,6] Kristin A. Persson*,[3,4] and Zhengcheng Zhang[1,*]

[1]Chemical Sciences and Engineering Division, Argonne National Laboratory, Lemont, IL 60439, USA

[2]Department of Chemistry, University of California, Berkeley, Berkeley, CA 94720, USA

[3]Department of Materials Science and Engineering, University of California, Berkeley, Berkeley, CA 94720, USA

[4]The Molecular Foundry, Lawrence Berkeley National Laboratory, Berkeley, CA 94720, USA

[5]Present address: School of Mechanical Engineering, Korea University, Seoul 02841, Korea

[6]Present address: Department of Chemistry, Inha University, Incheon 22212, Korea

Corresponding author

*E-mail: kapersson@lbl.gov; zzhang@anl.gov

**Abstract**

Sub-zero temperature performance is one of the most challenging aspects in lithium-ion batteries (LIBs). In conventional carbonate electrolytes at low temperatures (LT), there is insufficient thermal energy to efficiently cross the energy barrier associated with transporting $Li^+$ ion's across the electrolyte and into the anode. Although some fluorinated electrolytes with low $Li^+$ solvation energies have been proposed to improve LT performance, the working mechanism has remained ambiguous. Herein, we systematically investigate how the position and degree of fluorination of ethyl acetate (EA) influences its performance as a LT electrolyte solvent. We reveal that fluorination adjacent to the carbonyl group and a high degree of fluorination both impose a strong electron-withdrawing effect, resulting in low atomic charge on the solvating sites, low binding energies to $Li^+$ ions, low ionic conductivities, and poor solubilities at LT. A property balanced electrolyte based on trifluoroethyl acetate (EA-f) solvent showed excellent cycling performance and high C-rate capability at -20ºC and -40ºC, providing insight into the design of novel electrolytes for much needed LT LIBs.

## Introduction

Lithium-ion batteries (LIBs) are exploited in most portable electronics because of high energy/power density (long operation time), cyclability (life span), and simple manufacturing process (mass production).[1-4] However, with the spread of electric vehicles, low temperature operation of LIBs has become an issue due to the performance difference depending on regions and seasons.[5-6] Low temperature performance is considered to be the most challenging aspect in LIBs because the conventional electrolytes are based on ethylene carbonate (EC), an indispensable electrolyte solvent for stable solid-electrolyte-interphase (SEI) that also exhibits a high melting point of 34°C.[7-8] As temperatures drop, EC-based LIBs suffer from sharp drops in capacity and rate capability and severe degradation at low temperatures.[7-8]

The electrolytes in LIBs with graphite anodes normally include specific ratio of EC solvent since it can stabilize the graphite/electrolyte interface by ring-opening reduction, preventing the graphite from exfoliation by co-intercalation.[9-10] However, the high melting point (34°C) of EC impairs the low temperature performances as the electrolytes with a high portion of EC freeze under –20°C. To address the freezing problem, tertiary or quaternary carbonate systems with a low portion of EC were proposed,[11-12] but they still suffered from poor rate capability at low temperatures. In addition, to enhance rate capability at low temperatures, solvents with a high ionic conductivity such as ether,[13-18] ester,[19-25] or nitrile[8, 26-27] have been attempted as co-solvents. Among the functional groups, ester-based solvents have been actively studied due to the similar functionality with carbonates, but much lower melting points.

Recently, in the battery field, fluorinated electrolytes have received a tremendous attention from researchers due to their unexpected superior properties such as high oxidation stability, stable interface formation, and weak solvation energy.[28-30] Although some fluorinated ester-based electrolytes[31-34] such as methyl 3,3,3-trifluoropionate, or ethyl trifluoroacetate were

proposed for LIBs at low temperatures, the behind working mechanisms remain ambiguous. Previous studies on fluorinated ester electrolytes have studied the conventional electron-withdrawing effects of fluorination but provided little insight into the relation between the molecular structure and electrochemical performances.

In this paper, we systematically investigate the effect of the position and degree of fluorination on ethyl acetate (EA) as an electrolyte solvent. The terminal methyl groups of EA were replaced by trifluoro methyl groups, and compared from the view of physical, chemical, and electrochemical properties. We thoroughly analyzed their ionic conductivities, solvation structures ($^{7}$Li and $^{19}$F-nuclear magnetic resonance (NMR)), reduction potential (from density functional theory (DFT) and molecular dynamics (MD) simulations), solid-electrolyte interphase (SEI) layer, interfacial resistances, and electrochemical performances. From the various characterizations, we found an unexpected correlation; solvents fluorinated closer to the ester group possess poor physical properties such as low solubilities, ion clustering, and low ionic conductivities from extremely low binding energies. This defies the conventional understanding that weak solvation energy induced by fluorination is beneficial for improved electrochemical performances. Instead, the weakened physical properties impose a large overpotential during operation at low temperatures. This paper provides novel insights on design principles of fluorinated electrolytes for high performance LIBs at low temperatures.

## Results and Discussion

### Design principle of fluorinated ester-based electrolytes

Compared to the conventional Gen 2 electrolytes with ethylene carbonate and ethyl methyl carbonate co-solvent (1.2 M $LiPF_6$ in EC/EMC w/w=3/7), the state-of-the-art electrolyte for low temperature performances includes ethyl acetate (EA) solvent with fluoroethylene carbonate (FEC) co-solvent (**Figure 1**a). We reconfirmed the superiority of EA solvent compared to ethyl butyrate (EB) solvent (Figure S1). Although EA has a low melting point and high ionic conductivity, it exhibits a stronger binding to $Li^+$ ions than EMC due to the absence of an electron-withdrawing ester group, resulting in a higher desolvation energy. To decrease the desolvation energy, one of the limiting factors of $Li^+$ ion kinetics at low temperatures, we functionalized the terminal methyl group ($-CH_3$) to trifluoro methyl group ($-CF_3$), a strong electron-withdrawing group. In addition, the fluorination enhances high voltage stability with reduced the highest occupied molecular orbital (HOMO) levels, preventing the possible oxidation of hydrogen at high voltage. All the physical properties of solvents we used for this paper are included in Table S1.

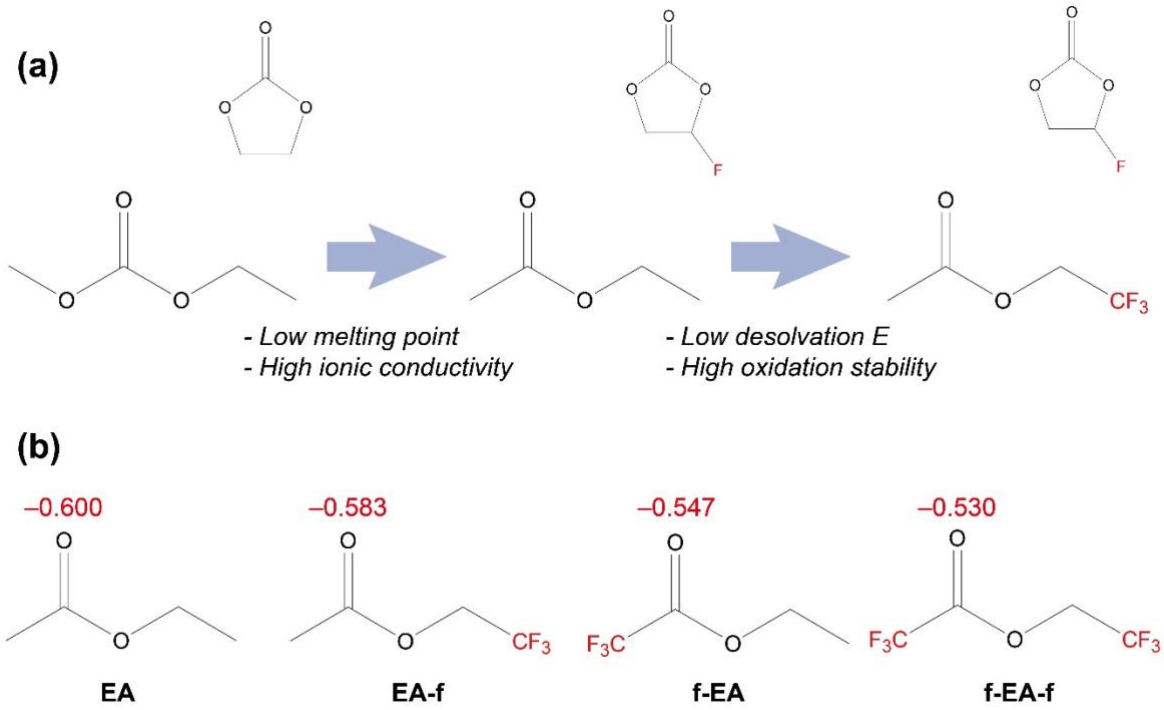


**Figure 1. (a)** Scheme of solvent design transition from carbonates to fluorinated esters. **(b)** Atomic charge analysis of carbonyl groups in EA, EA-f, f-EA, and f-EA-f.

In order to investigate the effect of the position and degree of fluorination, we compared different types of fluorinated ester solvents which are trifluoroethyl acetate (EA-f), ethyl trifluoroacetate (f-EA), and trifluoroethyl trifluoroacetate (f-EA-f) (Figure 1b). Atomic charge analysis via density functional theory (DFT) calculations reveals the electron-withdrawing effect of the -$CF_3$ groups. The atomic charge on the carbonyl group decreases in an order of EA, EA-f, f-EA, and f-EA-f. Since the electron-withdrawing effect in EA-f is shielded by an ether group, EA-f showed a higher atomic charge of –0.583 than that of –0.547 in f-EA. In the case of f-EA-f, it showed the lowest atomic charge of –0.530 due to the high degree of fluorination. This atomic charge analysis suggests different binding energies with $Li^+$ ions and different solvation structures in electrolytes.

**Solvation structures and ionic conductivities**

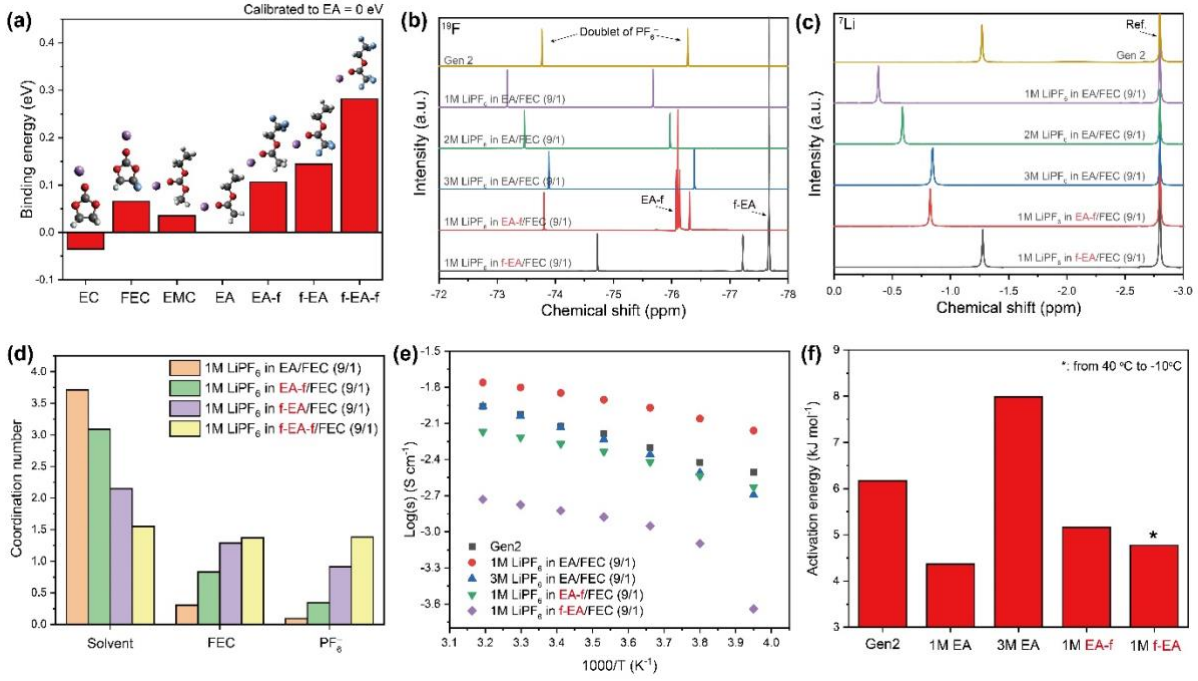


**Figure 2. (a)** Binding energies of each solvent with Li ion. The dielectric constant for implicit solvation model was 6.02, and they were calibrated to EA = 0 eV. **(b)** $^{19}$F- and **(c)** $^{7}$Li-NMR spectra of different electrolytes. **(d)** Coordination number in Li solvation sheath of different electrolytes from MD simulation. **(e)** Ionic conductivities of different electrolytes at various temperatures, and **(f)** their calculated activation energies ($E_a$) from plots (e).

To further appreciate the different electron-withdrawing effect, we calculated binding energies of each solvent with a $Li^+$ ion (**Figure 2**a). We applied implicit solvation effect for the calculations because $Li^+$ ions were chelated by f-EA and f-EA-f in gas phase, which is not feasible in electrolytes (Figure S2). The dielectric constant for implicit solvation effect was 6.02, and they were calibrated to EA = 0 eV. Note that a higher binding energy means relatively weaker binding to a Li ion. FEC had a higher binding energy (0.06 eV) than EC (–0.03 eV) due to the fluorination effect. In the case of EA-derivatives, EA-f, f-EA, and f-EA-f showed much higher binding energies of 0.11, 0.14, and 0.28 eV, respectively, than 0 eV of EA. The relative binding energies allow to expect solvation structures in co-solvent systems in a way

that solvent with lower binding energy would aggressively solvate Li ions. It is noteworthy that while FEC has a higher binding energy than EA, EA-derivatives have higher binding energies than FEC. A weaker interaction between $Li^+$ and the solvent correlates with a higher participation of FEC in the Li solvation shell in EA-derivative electrolytes, however the interaction between the co-solvents as well as entropic effects can influence the speciation of the Li solvation.

Understanding solvation structures in electrolytes is important because solvents coordinated with Li are likely to be reduced to form the SEI layer. The degree of ion-pairing also affects solubility and ionic conductivity. We used FEC co-solvent with 10 vol% since pure EA or EA-f solvents cannot stabilize the SEI layer (Figure S3). To analyze the solvation structures, we conducted nuclear magnetic resonance (NMR) characterization for each electrolyte. From the $^{19}$F-NMR spectra in Figure 2b, the doublet of $PF_6^-$ in 1 M $LiPF_6$ in EA/FEC (9/1) (EA electrolyte) was down-field shifted compared to Gen 2, indicating a lower ion-pair ratio. The peaks of $PF_6^-$ were gradually up-field shifted as the concentration increased, showing ion-clustering at high concentrations. While the peaks of $PF_6^-$ in 1 M $LiPF_6$ in EA-f/FEC (9/1) (EA-f electrolyte) were comparable to those in 3 M EA electrolyte or Gen 2, the peaks of $PF_6^-$ in 1 M $LiPF_6$ in f-EA/FEC (9/1) (f-EA electrolyte) were the most up-field shifted. f-EA-f electrolytes could not be measured because 1 M $LiPF_6$ was not soluble in f-EA-f/FEC (9/1) solvent even at room temperature.

The trend of peak shift was continued in the $^7$Li-NMR spectra (Figure 2c). As Li ions are solvated by solvents and anions, the corresponding Li peak shift can be considered as the sum of solvent and anion effects. Compared to –1.27 ppm in Gen 2, the Li peak in EA electrolyte was significantly down-field shifted to –0.39 ppm, implying a low portion of $PF_6^-$ in solvation structures. As the concentration increased, the Li peaks were up-field shifted due to the

participation of $PF_6^-$ in solvation structures. The Li peak in EA-f electrolyte was comparable to 3 M EA electrolyte, and they were still significantly down-field shifted to –0.82 ppm compared to Gen 2, indicating the weak binding of EA-f to $Li^+$ ions. The Li peak in f-EA electrolyte was similar to Gen 2 because of the sum of high portion of ion-pair and weak binding of f-EA. The solvation structure modification was reconfirmed by molecular dynamics (MD) simulations (Figure 2d). There is a strict trend in coordination number changes. In an order of EA, EA-f, f-EA, and f-EA-f, the coordination number of EA-derivative solvents decreased, and those of FEC or $PF_6^-$ increased due to the weakened binding energies of EA-derivative solvents. The representative solvation structures of each electrolyte were presented in Figure S4. This NMR characterization and MD simulation explain the modified solvation structures and energies in the EA-derivative electrolytes.

Ionic conductivities on various temperatures of different electrolytes were measured by electrochemical impedance spectroscopy (EIS) characterization using bulk electrolytes (Figure 2e and f). As known in the literature, the EA electrolyte had higher ionic conductivity than Gen 2, due to its lower viscosity and lower ion-pair ratio (high dissociation). As the concentration increased to 3 M, the ionic conductivities decreased with a high activation energy of 8.0 kJ $mol^{-1}$ because of the increased ion-pair ratio. In the case of EA-f electrolyte, the ionic conductivities were slightly lower than Gen 2, but they were high enough above 2.4 mS $cm^{-1}$ to sustain ion transport at low temperatures. In the case of f-EA electrolytes, however, the ionic conductivity was significantly low to 1.5 mS $cm^{-1}$ at room temperature, and it dropped to 0.2 mS $cm^{-1}$ at –20°C because $LiPF_6$ salt in electrolytes was precipitated under –20°C (Figure S5). This confirmed that weak binding energy of fluorinated solvents leads to trade-offs between desirable physical properties.

**SEI layers and interfacial resistances**

In our previous paper, we unveiled that the SEI layer plays a crucial role in rate capability and stability at low temperatures.[8] With that in mind, we added 0.1M LiDFOB to EA-f electrolyte as an additive to modify the SEI layer. The optimized electrolyte was 0.9 M $LiPF_6$ + 0.1 M LiDFOB in EA-f/FEC (9/1). The SEI layer formation can be seen in dQ/dV profiles of NMC622/graphite cells at a first charging step. In the **Figure 3**a, there was an EC reduction peak at 3.0 V in Gen 2. While there was a free FEC reduction peak at 2.7 V in EA electrolyte, $Li^+$-coordinated FEC was reduced earlier at 2.3 V in EA-f electrolyte. This is well matched with the coordination number change of FEC in electrolytes from MD simulations. In the EA-f electrolyte with LiDFOB additive, $DFOB^-$ was reduced earlier than $Li^+$-coordinated FEC, forming an ion-conductive SEI layer.[35-36] In the case of f-EA electrolyte, f-EA solvent was reduced earlier than FEC and showed high peaks at 2.6 and 2.7 V due to the high reduction potential (Figure S6).

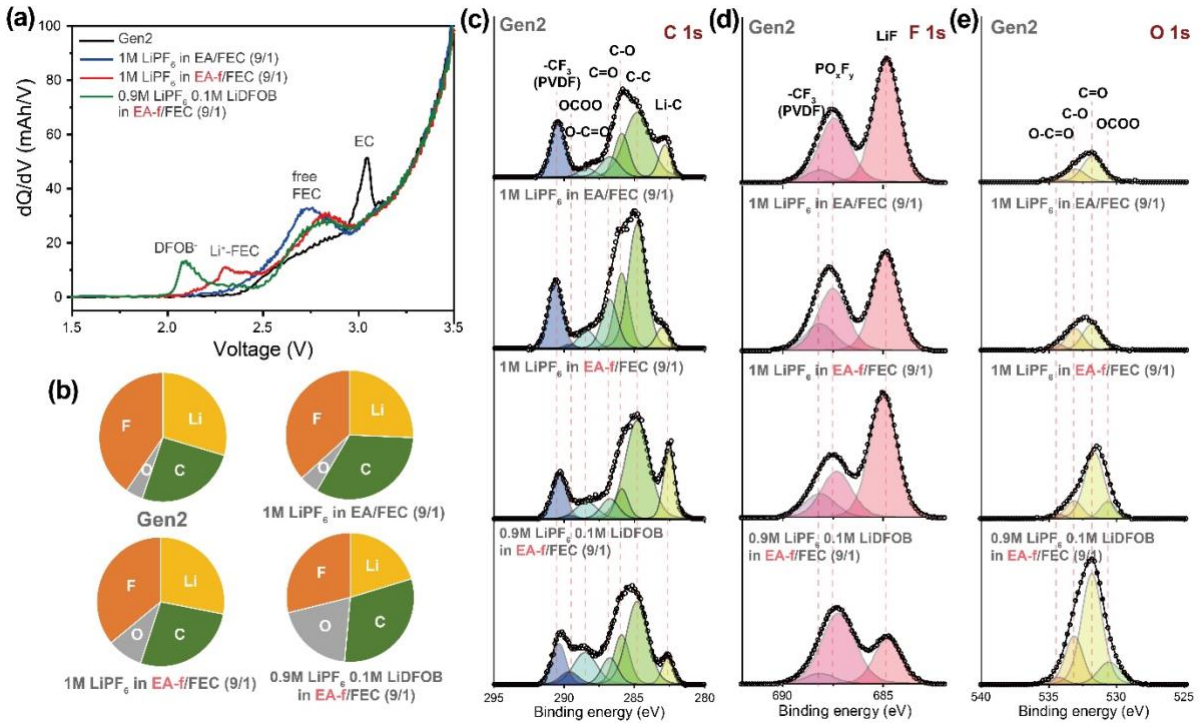


**Figure 3. (a)** dQ/dV profiles of graphite|NMC622 cells with different electrolytes during 1st charging. **(b)** Atomic ratio and XPS spectra of **(c)** C 1s, **(d)** F 1s, and **(e)** O 1s of cycled graphite

anodes after three formation cycles with different electrolytes.

In order to analyze the composition of SEI layers, we conducted X-ray photoelectron spectroscopy (XPS) characterization of graphite anodes in different electrolytes after three formation cycles. Based on the atomic ratio in Figure 3b we observe that the prevalence of Li and O were higher in the EA-f electrolyte than EA electrolytes, likely due to the reduction of $Li^+$-coordinated FEC. The fraction of O and C were further enlarged in EA-f electrolyte with LiDFOB additive, correlating to the active reduction of $DFOB^-$. Deconvolution of each element in the XPS spectra clarified the functional groups of reduction products. The participation of $Li^+$-coordinated FEC in the EA-f electrolyte caused a large peak from the C=O bond at 532 eV in O 1s spectra. The addition of LiDFOB further modified the SEI layer, leading to less LiF and more organic compounds, exhibiting C=O, OCOO, and O-C=O bonds. In the case of cathodes in the different electrolytes, there was no significant difference in the components on the surface (Figure S7).

To appreciate the effect of SEI layer and modified solvation structures to interfacial resistance, we measured temperature-dependent electrochemical impedance spectroscopy (EIS) for NMC622/graphite cells with different electrolytes at charged state to 3.7 V after three formation cycles (**Figure 4**). It is evident that as the temperature decreased, the total resistances increased due to the lower thermal energy of $Li^+$ ions for electrochemical reactions. While Gen 2 and EA electrolytes showed large total resistances to 365 Ω and 315 Ω at –20°C, respectively, EA-f electrolyte showed a much lower total resistance to 207 Ω at –20°C. In the case of the f-EA electrolyte, it showed the highest total resistance of 375 Ω at –20°C; presumably due to low $Li^+$ ion solubility and ionic conductivity at low temperatures (Figure S8).

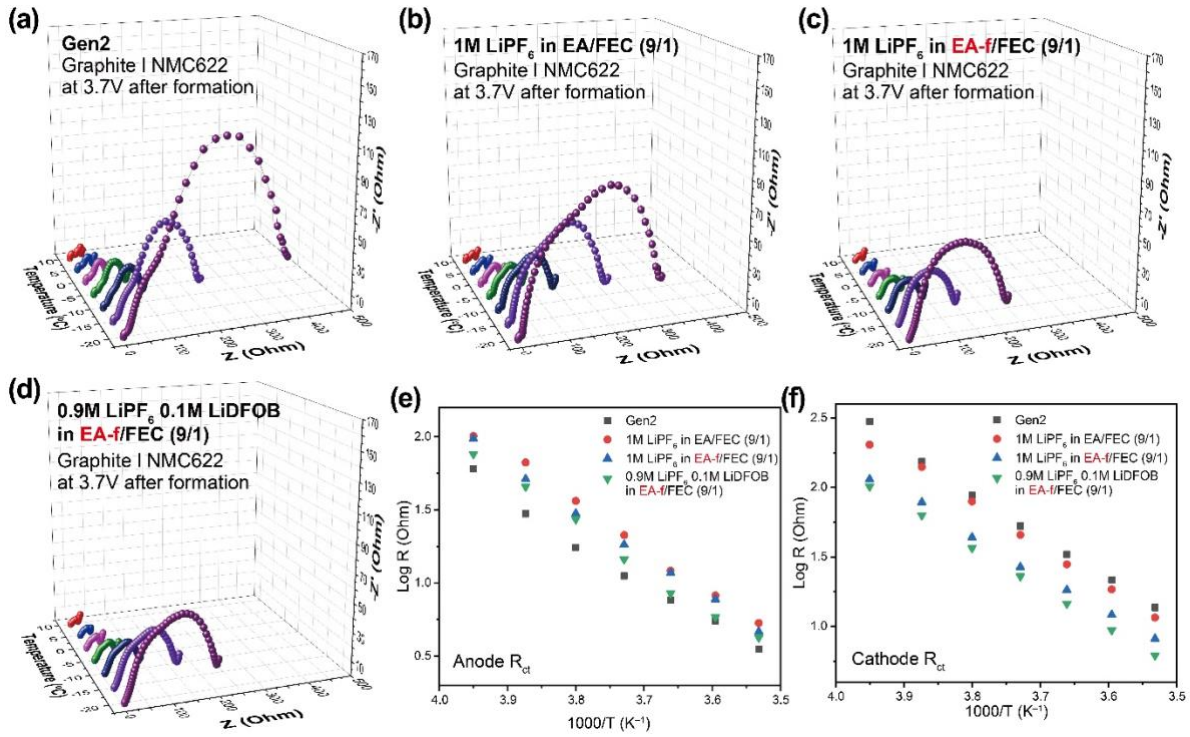


**Figure 4.** Nyquist plots of graphite|NMC622 cells with **(a)** Gen 2, **(b)** 1M $LiPF_6$ in EA/FEC (9/1), **(c)** 1M $LiPF_6$ in EA-f/FEC (9/1), and **(d)** 0.9M $LiPF_6$ 0.1M LiDFOB in EA-f/FEC (9/1) electrolyte at various temperatures. Arrhenius plots of **(e)** $R_{ct\text{-}anode}$, and **(f)** $R_{ct\text{-}cathode}$ fitted from (a-d).

To compare each resistance component contribution, we deconvoluted and extracted the charge transfer resistance at the anode ($R_{ct\text{-}anode}$) and charge transfer resistance at the cathode ($R_{ct\text{-}cathode}$) from the measured data, since those two components are known as limiting factors at low temperatures (Figure 4e and f). In the Arrhenius plot of $R_{ct\text{-}anode}$, Gen 2 showed the lowest resistance due to the ion-conductive SEI layer derived from EC reduction. While the EA electrolyte showed the highest resistance, EA-f and EA-f with LiDFOB additive showed relatively low resistances, likely due to the weaker solvation structure and modified SEI layer. In the case of $R_{ct\text{-}cathode}$, since there was no major difference in CEI layer composition, the

weaker solvation effect was directly observed. While EA electrolyte showed similar resistances to Gen 2, EA-f and EA-f with LiDFOB additive showed much smaller resistances. The temperature-dependent EIS measurement shows that the weak solvation structures in EA-f electrolytes improve the interfacial kinetics with the support of a modified SEI layer.

**Electrochemical performances**

One of the advantages of fluorination is high oxidation stability. To compare the stability of electrolytes, we conducted a voltage holding test of NMC622/graphite cells with different electrolytes with a voltage step from 4.4 V to 4.9 V for 10 hours in each step (**Figure 5**a). In the case of Gen 2, the leakage current sustained low up to 4.8 V, but started slightly increasing at 4.9 V. While the EA electrolyte showed a leakage current above 4.6 V, which rapidly increases at 4.9 V, EA-f and EA-f with LiDFOB additive maintained a low leakage current up to 4.9 V, indicating their superior oxidation stability. These results suggest the application of EA-f electrolytes to high voltage cathodes such as $LiMn_2O_4$ or $LiNi_{0.5}Mn_{1.5}O_4$.

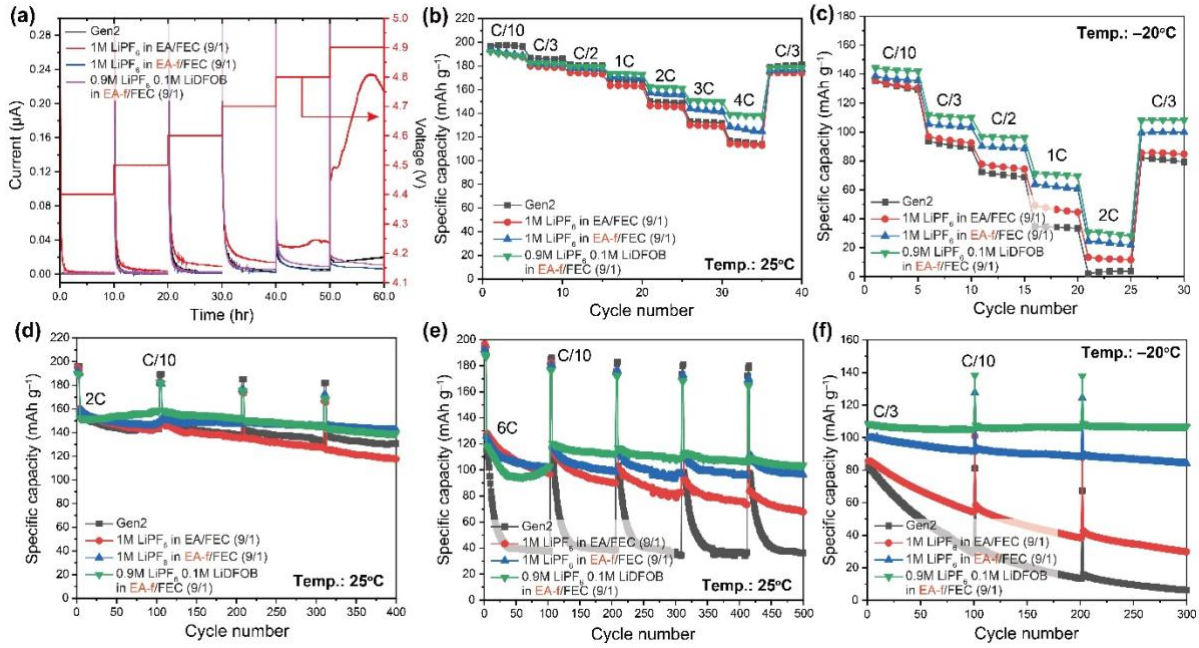


**Figure 5. (a)** Voltage holding test of graphite|NMC622 cells with different electrolytes from 4.4V to 4.9V. C-rate capability with different electrolytes at **(b)** 25°C and **(c)** –20°C. Cyclability at **(d)** 2C and **(e)** 6C rate with different electrolytes at 25°C. **(f)** Cyclability at C/3 rate with different electrolytes at –20°C.

We measured rate capability of electrolytes at 25°C and –20°C (Figure 5b and c). At room temperature, when various C-rates were applied from C/10 to 4C, Gen2 and EA electrolyte showed similar capacities of 116 and 113 mAh $g^{-1}$ at 4C, respectively. In contrast, EA-f electrolyte with LiDFOB additive showed the best rate capability and delivered 138 mAh $g^{-1}$ at 4C due to the weak solvation structure and modified SEI layer. As shown in the voltage profiles with normalized capacity (Figure S9), the overpotential evolution of Gen 2 approached 0.62 V at 4C, whereas that of EA-f electrolyte with LiDFOB additive maintained a low overpotential of 0.4 V at 4C.

When the temperature decreased to –20°C, the difference in rate capability between the electrolytes was further diverged. When a current of 1C was applied at –20°C, Gen 2 only

exhibited 33 mAh $g^{-1}$ capacity, while EA-f electrolyte with LiDFOB additive still maintained a high capacity of 70 mAh $g^{-1}$. In the voltage profiles of rate capabilities at –20°C (Figure S10) Gen 2 showed a high overpotential of 1.1 V at 1C while the EA-f electrolyte with LiDFOB additive remained at 0.77 V at 1C. To exclude the effect of high ion-pair ratio in electrolytes, we tested 2 M and 3 M EA electrolytes with same test conditions (Figure S11), and in the case of 3 M EA electrolyte, it showed better rate capability than Gen 2 at 25°C, but poor capability at –20°C due to the ion clustering and low ionic conductivity. Poor performance was also observed in f-EA electrolyte (Figure S12), reconfirming the trade-off relation between the weak solvation structure and electrochemical performance. Finally, superior rate capabilities of EA-f electrolytes were found in Li metal batteries (Figure S13), showing the best capacity retention at 25°C and –20°C.

Long-term cyclability at high C-rates and low temperatures is considered as one of the challenging aspects in LIBs. To prove the superiority of our electrolytes, we conducted long-term cycling tests with various conditions (Figure 5d-f). When a current of 2C was applied at 25°C, the EA electrolyte gradually decayed to a capacity retention of 73% after 400 cycles, while the EA-f electrolyte with LiDFOB additive showed the best capacity retention of 91% after 400 cycles. This trend continues at a further high current of 6C. While Gen 2 rapidly degraded to 34% within 50 cycles, the EA-f electrolyte with LiDFOB additive showed the best capacity retention of 85% even after 500 cycles. When a current of C/3 was applied at –20°C, Gen 2 and EA electrolytes showed a severe capacity degradation, corresponding to 7.5% and 34% capacity retention after 300 cycles, respectively. In stark contrast, the EA-f electrolyte with LiDFOB additive showed a negligible capacity loss and retained 97% capacity even after 300 cycles. This cycling test result reveals the superior stability of our electrolyte for fast charging and low temperature operations.

## Conclusions

In summary, we have systematically investigated the effect of the position and degree of fluorination in EA solvent on electrochemical performances. We reveal that a high degree of fluorination or fluorination close to ester group imposes more electron-withdrawing effect, resulting in low atomic charges, low binding energies to $Li^+$ ions, low ionic conductivities, and poor solubilities at low temperatures. Since interfacial resistance is governed by the kinetics of $Li^+$ ion desolvation, charge transfer across the SEI and ion conductivity, EA-f electrolyte shows the best electrochemical performance. EA-f effectively balances the property trade-offs associated with fluorination, outperforming both f-EA and f-EA-f. This study provides a deep insight on design principles of novel fluorinated electrolytes for LIBs operating at low temperatures.

**Experimental Section**

*Materials:* Ethyl acetate (EA), trifluoroethyl acetate (EA-f), ethyl trifluoroacetate (f-EA) and trifluoroethyl trifluoroacetate (f-EA-f) were purchased from Sigma Aldrich. All solvents used in this study were purified by vacuum distillation and then dried by adding 4 Å molecular sieves before use. Gen2 electrolyte is 1.2 M $LiPF_6$ in EC/EMC (3/7=w/w ratio). All electrodes were provided by Argonne's Cell Analysis, Modeling and Prototyping (CAMP) facility. The cathode NMC622 was composed of 90 wt% $LiNi_{0.6}Mn_{0.2}Co_{0.2}O_2$, 5 wt% polyvinylidene fluoride binder (PVdF, Solvay) and 5 wt% C45 conductive carbon casted on an aluminum foil with a mass loading of 9.78 mg/cm$^2$. The graphite anode was composed of 91.83 wt% Superior graphite (SLC1520P), 6 wt% PVdF binder (Kureha, 9300), 0.17 wt% oxalic acid additive, and 2 wt% C45 conductive carbon casted on a copper foil with a mass loading of 6.38 mg/cm$^2$. All electrodes were dried at 110$^o$C under vacuum for overnight. Celgard 2500 was used as the separator. The diameters of the cathode, anode and separator were 14, 15, and 16 mm, respectively.

*Electrochemical Measurements:* The electrochemical performance was evaluated by 2032 coin cells. The full cells were composed of NMC622 cathode and graphite anode with different electrolytes. The cell assembly was conducted in an argon-filled glovebox. All the galvanostatic cycling was performed at 2.7 ~ 4.4 V following three C/10 formation cycles using Neware battery tester. The electrochemical impedance spectroscopy (EIS) was obtained and fitted using a Solartron analyzer operated between 0.01 Hz and 1 MHz with amplitude of 10 mV.

*Characterization:* The cycled cells were disassembled in an argon-filled golvebox. The graphite and NMC622 electrodes were obtained at charged state to 3.7 V after three formation cycles with Gen 2, EA, EA-f, and LiDFOB-added EA-f electrolytes. The electrodes were rinsed

with dimethyl carbonate for Gen 2 cycled electrodes or EA for EA, EA-f, and LiDFOB-added EA-f electrolytes, and charaterized after vacuum dried. X-ray photoelectron spectroscopy (XPS) was conducted in the fixed analyzer transmission mode using an Al Kα radiation (hν = 1486.6 eV, 100 μm beam, 25 W) with $Ar^+$ and electron beam sample neutralization. XPS spectra were calibrated to the C-C bond at 284.7 eV. NMR

*DFT calculation:* Structure optimizations, binding energy and molecular orbital energy calculations were performed without symmetry restriction using the B3LYP hybrid density functional implemented in the GAUSSIAN 09 software package. The 6-311+G(d) basis sets were used for all the atoms. Frequency calculations of the same basis sets were conducted to obtain gibbs free energies of the solvents. The atomic charge was obtained from the natural bond orbital (NBO) analysis. The conductor-like polarization continuum model (CPCM) with the dielectric constant (ε=6.02) was used to implicitly take included solvent molecules into consideration. We calculated the reduction or oxidation potentials based on the following equation:

$$E\ (vs.\ Li/Li^+) = \frac{\Delta G}{-nF} - 1.4$$

,where $E$ is the formal potential, $\Delta G$ is the free energy of reaction, $n$ is the number of electrons transferred in the reaction, and $F$ is Faraday's constant. The potential compared $Li/Li^+$ was determined by subtracting 1.4 V, because the SHE is –4.4 V vs. vacuum and the potential of $Li/Li^+$ is –3.0 V vs. SHE.

*MD simlation*: We parameterized the system with the Sage force field[37] using the OpenForceField toolkit and calculated partial charges for the $PF_6^-$ with a Restrained Electrostatic Potential (RESP) fit using Antechamber.[38] The RESP calculation used a geometry

optimized structure calculated with Gaussian 16 at the B3LYP/aug-cc-pvdz level of theory. Ion partial charges were scaled to 80% of their initial value.[39]

We performed molecular dynamics calculations with the Open Molecular Mechanics (OpenMM) package.[40] A random initial configuration of the molecular system was generated with PACKMOL[41] followed by an energy minimization with conjugate gradient descent. Each simulation began with a 1 ns pressure equilibration in the NPT ensemble at 1 atm, 298 K. The system was then annealed by raising the temperature to 400 K, holding at 400 K, and then returning to 298 K, each for 1 ns. After this equilibration, the production part of the simulation ran for 5 ns. All solvation structure geometries and statistics were taken from the production run. We performed simulation setup with Pymatgen[42] and analysis of the molecular dynamics trajectories with MDAnalysis[43] and SolvationAnalysis[44].

**Reference**


1. Choi, J. W.; Aurbach, D., Promise and reality of post-lithium-ion batteries with high energy densities. *Nat. Rev. Mater.* **2016,** *1* (4), 16013.
2. Duffner, F.; Kronemeyer, N.; Tübke, J.; Leker, J.; Winter, M.; Schmuch, R., Post-lithium-ion battery cell production and its compatibility with lithium-ion cell production infrastructure. *Nat. Energy* **2021,** *6* (2), 123-134.
3. Li, M.; Lu, J.; Chen, Z.; Amine, K., 30 Years of Lithium-Ion Batteries. *Adv. Mater.* **2018,** *30* (33), 1800561.
4. Zeng, X.; Li, M.; Abd El-Hady, D.; Alshitari, W.; Al-Bogami, A. S.; Lu, J.; Amine, K., Commercialization of Lithium Battery Technologies for Electric Vehicles. *Adv. Energy Mater.* **2019,** *9* (27), 1900161.
5. Gupta, A.; Manthiram, A., Designing Advanced Lithium-Based Batteries for Low-Temperature Conditions. *Adv. Energy Mater.* **2020,** *10* (38), 2001972.
6. Hou, J.; Yang, M.; Wang, D.; Zhang, J., Fundamentals and Challenges of Lithium Ion Batteries at Temperatures between −40 and 60 °C. *Adv. Energy Mater.* **2020,** *10* (18), 1904152.
7. Zhu, G.; Wen, K.; Lv, W.; Zhou, X.; Liang, Y.; Yang, F.; Chen, Z.; Zou, M.; Li, J.; Zhang, Y.; He, W., Materials insights into low-temperature performances of lithium-ion batteries. *J. Power Sources* **2015,** *300*, 29-40.
8. Yoo, D.-J.; Liu, Q.; Cohen, O.; Kim, M.; Persson, K. A.; Zhang, Z., Understanding the Role of SEI Layer in Low-Temperature Performance of Lithium-Ion Batteries. *ACS Appl. Mater. Interfaces* **2022,** *14* (9), 11910-11918.
9. Song, H.-Y.; Jeong, S.-K., Investigating continuous co-intercalation of solvated lithium ions and graphite exfoliation in propylene carbonate-based electrolyte solutions. *J. Power Sources* **2018,** *373*, 110-118.
10. Ming, J.; Cao, Z.; Wu, Y.; Wahyudi, W.; Wang, W.; Guo, X.; Cavallo, L.; Hwang, J.-Y.; Shamim, A.; Li, L.-J.; Sun, Y.-K.; Alshareef, H. N., New Insight on the Role of Electrolyte Additives in Rechargeable Lithium Ion Batteries. *ACS Energy Lett.* **2019,** *4* (11), 2613-2622.
11. Liao, X.-Z.; Ma, Z.-F.; Gong, Q.; He, Y.-S.; Pei, L.; Zeng, L.-J., Low-temperature performance of LiFePO4/C cathode in a quaternary carbonate-based electrolyte. *Electrochem. commun.* **2008,** *10* (5), 691-694.
12. Smart, M. C.; Ratnakumar, B. V.; Whitcanack, L. D.; Chin, K. B.; Surampudi, S.; Croft, H.; Tice, D.; Staniewicz, R., Improved low-temperature performance of lithium-ion cells with quaternary carbonate-based electrolytes. *J. Power Sources* **2003,** *119-121*, 349-358.
13. Carbone, L.; Gobet, M.; Peng, J.; Devany, M.; Scrosati, B.; Greenbaum, S.; Hassoun, J., Comparative Study of Ether-Based Electrolytes for Application in Lithium–Sulfur Battery. *ACS Appl. Mater. Interfaces* **2015,** *7* (25), 13859-13865.
14. Zhao, Q.; Liu, X.; Zheng, J.; Deng, Y.; Warren, A.; Zhang, Q.; Archer, L., Designing electrolytes with polymerlike glass-forming properties and fast ion transport at low temperatures. *Proc. Natl. Acad. Sci. U.S.A.* **2020,** *117* (42), 26053-26060.
15. Xu, J.; Wang, X.; Yuan, N.; Ding, J.; Qin, S.; Razal, J. M.; Wang, X.; Ge, S.; Gogotsi, Y., Extending the low temperature operational limit of Li-ion battery to −80 °C. *Energy Storage Mater.* **2019,** *23*, 383-389.
16. Ramasamy, H. V.; Kim, S.; Adams, E. J.; Rao, H.; Pol, V. G., A novel cyclopentyl methyl ether electrolyte solvent with a unique solvation structure for subzero (−40 °C) lithium-ion batteries. *Chem. Commun.* **2022,** *58* (33), 5124-5127.
17. Zhang, X.; Zou, L.; Xu, Y.; Cao, X.; Engelhard, M. H.; Matthews, B. E.; Zhong, L.; Wu, H.; Jia, H.; Ren, X.; Gao, P.; Chen, Z.; Qin, Y.; Kompella, C.; Arey, B. W.; Li, J.; Wang,

D.; Wang, C.; Zhang, J.-G.; Xu, W., Advanced Electrolytes for Fast-Charging High-Voltage Lithium-Ion Batteries in Wide-Temperature Range. *Adv. Energy Mater.* **2020,** *10* (22), 2000368.
18. Qin, Y.; Ren, Z.; Wang, Q.; Li, Y.; Liu, J.; Liu, Y.; Guo, B.; Wang, D., Simplifying the Electrolyte Systems with the Functional Cosolvent. *ACS Appl. Mater. Interfaces* **2019,** *11* (31), 27854-27861.
19. Smart, M. C.; Ratnakumar, B. V.; Surampudi, S., Use of Organic Esters as Cosolvents in Electrolytes for Lithium-Ion Batteries with Improved Low Temperature Performance. *J. Electrochem. Soc.* **2002,** *149* (4), A361.
20. Herreyre, S.; Huchet, O.; Barusseau, S.; Perton, F.; Bodet, J. M.; Biensan, P., New Li-ion electrolytes for low temperature applications. *J. Power Sources* **2001,** *97-98*, 576-580.
21. Sazhin, S. V.; Khimchenko, M. Y.; Tritenichenko, Y. N.; Lim, H. S., Performance of Li-ion cells with new electrolytes conceived for low-temperature applications. *J. Power Sources* **2000,** *87* (1), 112-117.
22. Lu, W.; Xie, K.; Chen, Z.; Xiong, S.; Pan, Y.; Zheng, C., A new co-solvent for wide temperature lithium ion battery electrolytes: 2,2,2-Trifluoroethyl n-caproate. *J. Power Sources* **2015,** *274*, 676-684.
23. Smith, K. A.; Smart, M. C.; Prakash, G. K. S.; Ratnakumar, B. V., Electrolytes Containing Fluorinated Ester Co-Solvents for Low-Temperature Li-Ion Cells. *ECS Trans.* **2008,** *11* (29), 91-98.
24. Lu, W.; Xie, K.; Pan, Y.; Chen, Z.-x.; Zheng, C.-m., Effects of carbon-chain length of trifluoroacetate co-solvents for lithium-ion battery electrolytes using at low temperature. *J. Fluor. Chem.* **2013,** *156*, 136-143.
25. Smart, M. C.; Ratnakumar, B. V.; Chin, K. B.; Whitcanack, L. D., Lithium-Ion Electrolytes Containing Ester Cosolvents for Improved Low Temperature Performance. *J. Electrochem. Soc.* **2010,** *157* (12), A1361.
26. Cho, Y.-G.; Kim, Y.-S.; Sung, D.-G.; Seo, M.-S.; Song, H.-K., Nitrile-assistant eutectic electrolytes for cryogenic operation of lithium ion batteries at fast charges and discharges. *Energy Environ. Sci.* **2014,** *7* (5), 1737-1743.
27. Chen, J.; Vatamanu, J.; Xing, L.; Borodin, O.; Chen, H.; Guan, X.; Liu, X.; Xu, K.; Li, W., Improving Electrochemical Stability and Low-Temperature Performance with Water/Acetonitrile Hybrid Electrolytes. *Adv. Energy Mater.* **2020,** *10* (3), 1902654.
28. Hu, L.; Zhang, Z.; Amine, K., Fluorinated electrolytes for Li-ion battery: An FEC-based electrolyte for high voltage LiNi0.5Mn1.5O4/graphite couple. *Electrochem. commun.* **2013,** *35*, 76-79.
29. Tornheim, A.; Sahore, R.; He, M.; Croy, J. R.; Zhang, Z., Preformed Anodes for High-Voltage Lithium-Ion Battery Performance: Fluorinated Electrolytes, Crosstalk, and the Origins of Impedance Rise. *J. Electrochem. Soc.* **2018,** *165* (14), A3360-A3368.
30. Zhang, Z.; Hu, L.; Wu, H.; Weng, W.; Koh, M.; Redfern, P. C.; Curtiss, L. A.; Amine, K., Fluorinated electrolytes for 5 V lithium-ion battery chemistry. *Energy Environ. Sci.* **2013,** *6* (6), 1806-1810.
31. Holoubek, J.; Yu, M.; Yu, S.; Li, M.; Wu, Z.; Xia, D.; Bhaladhare, P.; Gonzalez, M. S.; Pascal, T. A.; Liu, P.; Chen, Z., An All-Fluorinated Ester Electrolyte for Stable High-Voltage Li Metal Batteries Capable of Ultra-Low-Temperature Operation. *ACS Energy Lett.* **2020,** *5* (5), 1438-1447.
32. Sato, K.; Yamazaki, I.; Okada, S.; Yamaki, J.-i., Mixed solvent electrolytes containing fluorinated carboxylic acid esters to improve the thermal stability of lithium metal anode cells. *Solid State Ion.* **2002,** *148* (3), 463-466.
33. Yang, Y.; Li, P.; Wang, N.; Fang, Z.; Wang, C.; Dong, X.; Xia, Y., Fluorinated carboxylate ester-based electrolyte for lithium ion batteries operated at low temperature. *Chem.*

*Commun.*
**2020,** *56* (67), 9640-9643.
34. An, K.; Tran, Y. H. T.; Kwak, S.; Han, J.; Song, S.-W., Design of Fire-Resistant Liquid Electrolyte Formulation for Safe and Long-Cycled Lithium-Ion Batteries. *Adv. Funct. Mater.* **2021,** *31* (48), 2106102.
35. Jones, J.-P.; Smart, M. C.; Krause, F. C.; Bugga, R. V., The Effect of Electrolyte Additives upon Lithium Plating during Low Temperature Charging of Graphite-LiNiCoAlO<sub>2</sub> Lithium-Ion Three Electrode Cells. *J. Electrochem. Soc.* **2020,** *167* (2), 020536.
36. Xu, M.; Zhou, L.; Hao, L.; Xing, L.; Li, W.; Lucht, B. L., Investigation and application of lithium difluoro(oxalate)borate (LiDFOB) as additive to improve the thermal stability of electrolyte for lithium-ion batteries. *J. Power Sources* **2011,** *196* (16), 6794-6801.
37. Qiu, Y.; Smith, D. G. A.; Boothroyd, S.; Jang, H.; Hahn, D. F.; Wagner, J.; Bannan, C. C.; Gokey, T.; Lim, V. T.; Stern, C. D.; Rizzi, A.; Tjanaka, B.; Tresadern, G.; Lucas, X.; Shirts, M. R.; Gilson, M. K.; Chodera, J. D.; Bayly, C. I.; Mobley, D. L.; Wang, L.-P., Development and Benchmarking of Open Force Field v1.0.0—the Parsley Small-Molecule Force Field. *J. Chem. Theory Comput.* **2021,** *17* (10), 6262-6280.
38. Wang, J.; Wang, W.; Kollman, P. A.; Case, D. A., Automatic atom type and bond type perception in molecular mechanical calculations. *J. Mol. Graph. Model.* **2006,** *25* (2), 247-260.
39. Chaudhari, M. I.; Nair, J. R.; Pratt, L. R.; Soto, F. A.; Balbuena, P. B.; Rempe, S. B., Scaling Atomic Partial Charges of Carbonate Solvents for Lithium Ion Solvation and Diffusion. *J. Chem. Theory Comput.* **2016,** *12* (12), 5709-5718.
40. Eastman, P.; Swails, J.; Chodera, J. D.; McGibbon, R. T.; Zhao, Y.; Beauchamp, K. A.; Wang, L.-P.; Simmonett, A. C.; Harrigan, M. P.; Stern, C. D.; Wiewiora, R. P.; Brooks, B. R.; Pande, V. S., OpenMM 7: Rapid development of high performance algorithms for molecular dynamics. *PLoS Comput. Biol.* **2017,** *13* (7), e1005659.
41. Martínez, L.; Andrade, R.; Birgin, E. G.; Martínez, J. M., PACKMOL: A package for building initial configurations for molecular dynamics simulations. *J. Comput. Chem.* **2009,** *30* (13), 2157-2164.
42. Ong, S. P.; Richards, W. D.; Jain, A.; Hautier, G.; Kocher, M.; Cholia, S.; Gunter, D.; Chevrier, V. L.; Persson, K. A.; Ceder, G., Python Materials Genomics (pymatgen): A robust, open-source python library for materials analysis. *Comput. Mater. Sci.* **2013,** *68*, 314-319.
43. R. J. Gowers, M. Linke, J. Barnoud, T. J. E. Reddy, M. N. Melo, S. L. Seyler, D. L. Dotson, J. Domanski, S. Buchoux, I. M. Kenney, and O. Beckstein. MDAnalysis: A Python package for the rapid analysis of molecular dynamics simulations. In S. Benthall and S. Rostrup, editors, *Proceedings of the 15th Python in Science Conference*, pages 98-105, Austin, TX, 2016. SciPy, doi:10.25080/majora-629e541a-00e.
44. Cohen, O. SolvationAnalysis v0.1.2 (2021). https://pypi.org/project/solvation-analysis/